Theory of a zone-boundary collective state in Al: A model calculation

K. Sturm
Institut für Festkörperforschung der Kernforschungsanlage Jülich, D-5170 Jülich, West Germany

L. E. Oliveira
Instituto de Física, Universidade Estadual de Campinas (UNICAMP), Campinas 13100, São Paulo, Brazil

(Received 25 June 1984)

A two-band model, which previously was used successfully to evaluate the optical absorption in Al, is applied to derive the $\vec{k}$- and ω-dependent dielectric function $\epsilon_M(\vec{k},\omega)$ for $\vec{k}$ parallel to the [100] direction with use of degenerate perturbation theory. Within the nearly-free-electron approximation, it is shown that a pair of (200) Bragg planes gives rise to another pole in the energy-loss function $\mathrm{Im}[-1/\epsilon]$ and hence to a collective mode. Both the dispersion of the mode throughout the first Brillouin zone and the strength of the mode are evaluated and are found to agree very well with electron-energy-loss spectroscopy data. A detailed discussion of the nature of this mode is given. The mode is of the same origin as the so-called zone-boundary collective state (ZBCS) first proposed by Foo and Hopfield in Na. Comparison is made with a numerical calculation of $\epsilon_M(\vec{k},\omega)$ by Singhal for some discrete $\vec{k}$ values. The general importance of the ZBCS for the understanding of the energy-loss spectrum and for more complicated systems is pointed out.

I. INTRODUCTION

The prototype of a collective mode in the electronic excitation spectrum of metals and semiconductors is the "classical" plasmon. Most of our theoretical understanding of this mode is based on the free-electron model and the random-phase approximation (RPA). The framework in which this collective mode is discussed is the macroscopic dielectric function $\epsilon_M(\vec{k},\omega)$. For a free-electron gas treated in the RPA, $\epsilon_M(\vec{k},\omega)$ is the well-known Lindhard dielectric function $\epsilon_L(k,\omega)$. One of the standard methods to measure the plasmon is the inelastic scattering of fast electrons by a thin metal (or semiconductor) film, known as electron-energy-loss spectroscopy (EELS).[1] The doubly differential scattering cross section is proportional to the (energy-) loss function $\mathrm{Im}[-1/\epsilon_M(\vec{k},\omega)]$, where $\vec{k}$ and ω ($\hbar=1$) are the momentum transfer and energy transfer of the incoming electron to the system in question. In the system $\vec{k}$ and ω are the momentum and the energy of the elementary excitations. Theoretically, for fixed $\vec{k}$, sharp structures in the scattering cross sections are observed when the loss function $\mathrm{Im}[-1/\epsilon_M(\vec{k},\omega)]$ has a pole close to the real axis in the complex ω plane. For a free-electron gas in the RPA it is exactly from this condition that one obtains the plasmon $\omega_p(k)$ as a sharp (undamped) excitation for $k<k_c$. No further sharp structures are contained in $\mathrm{Im}[-1/\epsilon_L(k,\omega)]$; there are, however, relative maxima within the particle-hole excitation spectrum as is shown in Fig. 1 for an electron density appropriate for Al.

The natural question to ask is the following: In which way is the spectrum of $\mathrm{Im}[-1/\epsilon_M(\vec{k},\omega)]$ modified when a weak crystal potential is taken into account within the nearly-free-electron pseudopotential approach, for example? With respect to the collective excitations there are essentially two modifications:

(i) The plasmon is modified in various ways.[2] Due to real interband transitions the plasmon can decay even within the RPA. In this way most of the observed characteristic linewidth can be explained. Virtual interband transitions lead to a small $\vec{k}$-dependent shift of the plasmon energy from the free-electron value. It explains the anisotropy of the plasmon dispersion observed on single-crystal materials.

(ii) A new collective mode, the so-called zone-boundary collective state (ZBCS), appears, which is a consequence of the periodic modulation of the electron density resulting from the Bloch character of the single-electron states.

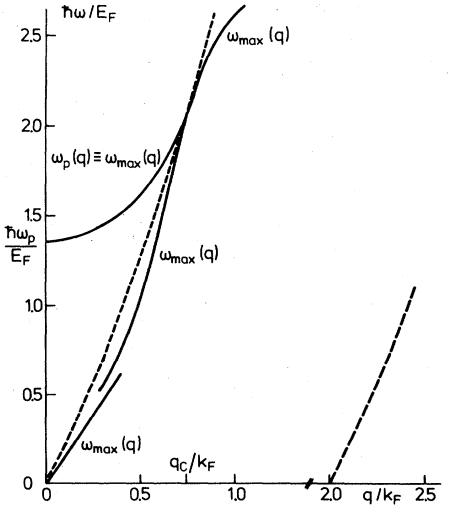

FIG. 1. Excitation spectrum of the free-electron gas with density appropriate to aluminum. Solid lines indicate the plasmon dispersion and relative maxima of the Lindhard loss function within the particle-hole excitation spectrum bounded by dashed lines.

The term "zone-boundary collective state" was first mentioned in a paper by Foo and Hopfield[3] on the optical properties of Na. They discussed the possible influence of this mode on the optical properties due to electron-phonon coupling. So far, this mode has not been observed directly by EELS in Na.

The first experimental evidence for the existence of such a mode in Al was found by Boersch *et al.*[4] In 1975, Petri and Otto[5] were the first to measure the $\vec{k}$ dependence of this energy-loss peak on single-crystal Al for $\vec{k}$ parallel to the [100] direction. Shortly after their measurements, the mode was also observed on single-crystal Al by Urner-Wille.[6] A particularly detailed experimental investigation was carried out by Chen and Silcox.[7] They demonstrated the existence of this mode along the [100] direction throughout the first Brillouin zone (BZ) as a rather well-defined mode and could also measure the $\vec{k}$ dependence of the (relative) strength of the mode (i.e., of the residue of the pole in the loss function). Quite opposite to the observed decrease of the strength of the plasmon pole with increasing $\vec{k}$ they observed a strong increase of the strength of the ZBCS with increasing $\vec{k}$.

Petri and Otto[5] pointed out the connection of the observed mode in Al with the conjectured mode in Na by Foo and Hopfield,[3] but no quantitative comparison was possible. After the work of Petri and Otto,[5] Singhal[8] calculated the energy-loss function for Al from a 15×15 microscopic dielectric matrix for four discrete $\vec{k}$ vectors parallel to the [100] direction [$\vec{k}$ in units of $\pi/2a$: (1,0,0), (2,0,0), (3,0,0), (4,0,0)]. The positions of the prominent peaks are in very good agreement with the dispersion found by Petri and Otto,[5] and by Chen and Silcox.[7] Qualitatively an increase of the intensity of the peaks with increasing $\vec{k}$ is theoretically observed. Unfortunately, $\mathrm{Re}\epsilon_M(\vec{k},\omega)$ and $\mathrm{Im}\epsilon_M(\vec{k},\omega)$ were not shown in the paper. Therefore the true nature of the peaks is not directly clear in the sense that it could either be a relative maximum in the particle-hole excitation spectrum or a genuine collective mode. Furthermore, the dispersion of the mode for small $\vec{k}$ was not theoretically obtained since Singhal's calculations were performed for four discrete values only, the smallest value being $|\vec{k}|=0.39$ Å^{-1}.

Boersch *et al.*[4] pointed out the connection of the peak in the loss function near 1.5 eV with the peak in the optical absorption at about the same energy. Ashcroft and Sturm[9] showed that the peak in the optical absorption is associated with interband transitions between single-particle states at the zone boundary. The effect could be quantitatively described by a two-band model using degenerate perturbation theory within a nearly-free-electron (NFE) pseudopotential approach. Using the results of Ashcroft and Sturm it is straightforward to show that these strong interband transitions lead to another pole in the loss function[2] at 1.48 eV as found by Boersch *et al.*[4] The purpose of the present work[10] is to extend the calculation within the two-band model to obtain $\epsilon_M(\vec{k},\omega)$ for finite $\vec{k}$. We are thus able to elucidate the true nature of the zone-boundary mode as a collective mode and obtain the dispersion of this mode along the [100] direction throughout the first BZ. The result is shown in Fig. 2. The dash-dotted line is the dispersion $\omega_{\mathrm{ZBCS}}(\vec{k})$ for $\vec{k}$ parallel to the [100] direction. The overall agreement between theory and experiment is very good. For very small

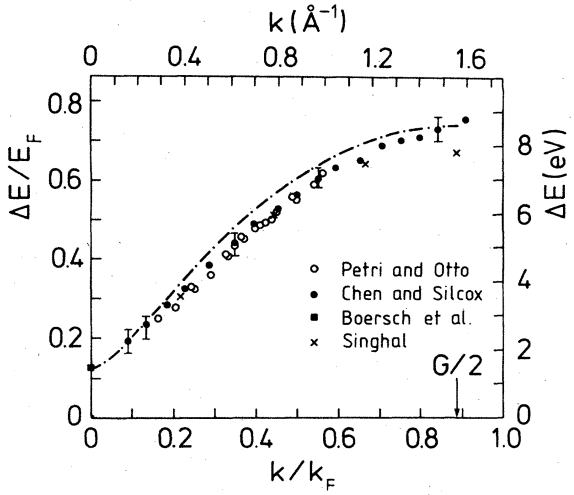

FIG. 2. Peak positions in the energy-loss function: comparison between theories and experiments. Present theory: dispersion of the (200) ZBCS (dash-dotted line); Singhal's theory: crosses (taken from Table I of Singhal's work[8]); open circles correspond to EELS data by Petri and Otto[5]; solid circles: EELS data by Chen and Silcox[7]; solid square: EELS data by Boersch *et al.*[4]

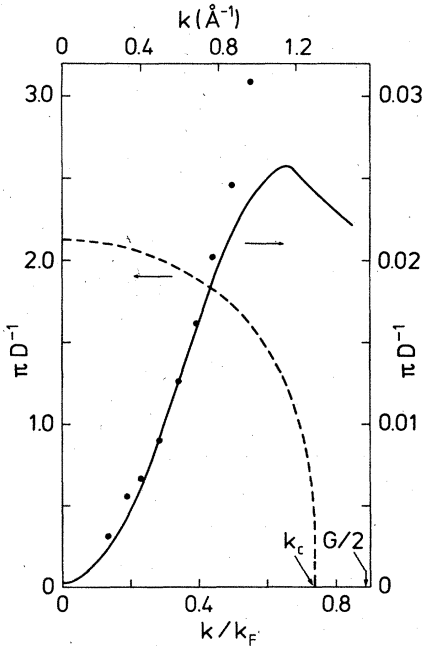

FIG. 3. Strength of the (200) ZBCS: comparison between theory (solid line) and EELS data from Chen and Silcox[7] (solid circles). Experimental points are normalized to theory at $k=0.6$ Å^{-1}. Also shown is the strength of the plasmon mode (dashed line). Notice different scales on vertical axes. $[\pi D^{-1}\equiv\pi\,|\,\partial\,\mathrm{Re}\epsilon_M(\vec{k},\omega)/\partial\omega\,|^{-1}_{\omega_c(\vec{k})}$, with $\omega_c(\vec{k})=\omega_p(\vec{k})$ for the plasmon and $\omega_c(\vec{k})=\omega_{\mathrm{ZBCS}}(\vec{k})$ for the ZBCS.]

$\vec{k}$ a quadratic dispersion is found as expected for symmetry reasons. The theoretical points (crosses) by Singhal[8] are systematically lower than our results. We shall comment on that later. In Fig. 3, the strength of the zone-boundary collective mode is compared with the experimental points obtained by Chen and Silcox[7] (solid circles). The dashed curve illustrates the completely different behavior of the plasmon. The discrepancy between theory and experiment for large $\vec{k}$ is very likely to be due to multiple scattering effects on the fast incoming electron. It can suffer both an inelastic scattering event with a momentum transfer $\vec{k}$ and an elastic scattering event with a momentum transfer of a reciprocal-lattice vector $\vec{G}\neq\vec{0}$, giving rise to a loss spectrum centered around $\vec{G}\neq\vec{0}$, which overlaps the loss spectrum at $\vec{G}=\vec{0}$ for large k. Such an effect was observed for the plasmon in Si by Stiebling and Raether.[11]

Another motivation for the present work came from a recent controversy on the plasmon dispersion in Al by Möller and Otto[12] and by Sturm.[13] The experimentally observed dispersion constant α_{expt} of the small k quadratic dispersion law[14]

$$\omega_p(k)=\omega_p(0)+2\alpha k^2+\cdots$$

deviates appreciably from the predicted value

$$\alpha_{\text{RPA}}=\frac{3}{5}\frac{1}{\omega_p}=0.45\ .$$

Corrections due to exchange and correlation effects beyond the RPA (see, for example, Vashishta and Singwi[15] and Iwamoto *et al.*[16]) tend to reduce α but not to such a degree as to bring it into agreement with the observed dispersion. In an attempt to resolve this discrepancy, Möller and Otto,[12] following an earlier conjecture of Petri and Otto[5] that the low-lying strong interband transition in Al might strongly influence the small-k plasmon dispersion, designed a simple model to demonstrate this. Their model calculation was criticized by Sturm,[13] who denied such a strong influence on account of his own theoretical investigation of the influence of the weak pseudopotential on the plasmon dispersion within standard nondegenerate perturbation theory. In their reply, Möller and Otto[12] requested that "the nonexisting influence of the low-lying interband transitions on the plasmon dispersion should be substantiated by calculations with the microscopic theory of dielectric properties yielding both the plasmon and the interband loss peak dispersion".

The present model calculation exactly satisfies this requirement. It can be used to calculate the dispersion of the (200) zone-boundary collective mode and to study the influence of interband transitions on the plasmon dispersion. The calculation confirms the result of nondegenerate perturbation theory that interband transitions have negligible influence on the small-k plasmon dispersion constant α.

II. THE TWO-BAND MODEL

First-principle calculations of $\epsilon_M(\vec{k},\omega)$, in particular for $\vec{k}\neq\vec{0}$ (and $\omega\neq0$), for real systems are still rather scarce even within the RPA because of the numerical complexity of the problem. Therefore, approximate calculations which can be performed analytically or partially analytically are very valuable and offer a more direct understanding of the properties.

The evaluation of the optical properties of polyvalent metals within the NFE pseudopotential approach using degenerate perturbation theory by Ashcroft and Sturm[9] is a typical example of such an approximate theory. Application of this theory to Al yielded quantitative agreement with experiment and the accuracy of the perturbation theory was tested against a numerical calculation by Dresselhaus *et al.*[17] In this approach, the effect of each of the 14 Bragg planes bounding the first BZ was treated separately in a two-band model by degenerate perturbation theory in order to construct the band structure and Bloch states. The contribution from (direct) interband transitions to the optical absorption $\text{Re}\sigma(\omega)$ is evaluated for each Bragg plane and the total interband absorption is obtained by a superposition of the individual contributions. The final result can be presented in the following form:

$$\text{Re}\sigma(\omega)=\frac{1}{3\pi}\sum_G\frac{|V_G|^2G^4}{\omega^3}\frac{\text{Im}\tilde{\epsilon}_L(G,\omega)}{[1-(2V_G/\omega)^2]^{1/2}}\Theta(\omega-2|V_G|)\ , \tag{2.1}$$

where the summation extends over the sets of eight equivalent $\{G_{111}\}$ and of six equivalent $\{G_{200}\}$ reciprocal-lattice vectors. $\tilde{\epsilon}_L(G,\omega)$ is the well-known Lindhard dielectric function with a minor modification as exhibited below:[14]

$$\text{Im}\tilde{\epsilon}_L(G,\omega)=\begin{cases}\dfrac{3\pi}{16}\dfrac{\omega_p^2\omega}{G^3} & \text{for } 0<\omega<\tilde{\omega}_1(G) \text{ and } 0<G<2\ ,\\ \dfrac{3\pi}{64}\dfrac{\omega_p^2}{G^5}[\tilde{\omega}_1(G)+\omega][\tilde{\omega}_2(G)-\omega] & \text{for } \tilde{\omega}_1(G)<\omega<\tilde{\omega}_2(G)\ ,\\ 0 \text{ otherwise}\ . & \end{cases} \tag{2.2}$$

The minor modification consists in replacing in the free-electron formula $\omega_{1,2}(G)=2G\mp G^2$ by

$$\tilde{\omega}_{1,2}(G)=2(G^2E_F+|V_G|^2)^{1/2}\mp G^2\ .$$

Obviously $\tilde{\omega}_1(G)$ and $\tilde{\omega}_2(G)$ differ only little from $\omega_1(G)$ and $\omega_2(G)$. E_F is the true Fermi energy that differs little from 1 in our units. The square-root singularity in (2.1) gives rise to the strong peak in $\text{Re}\sigma(\omega)$ near $\omega=2|V_{200}|$.

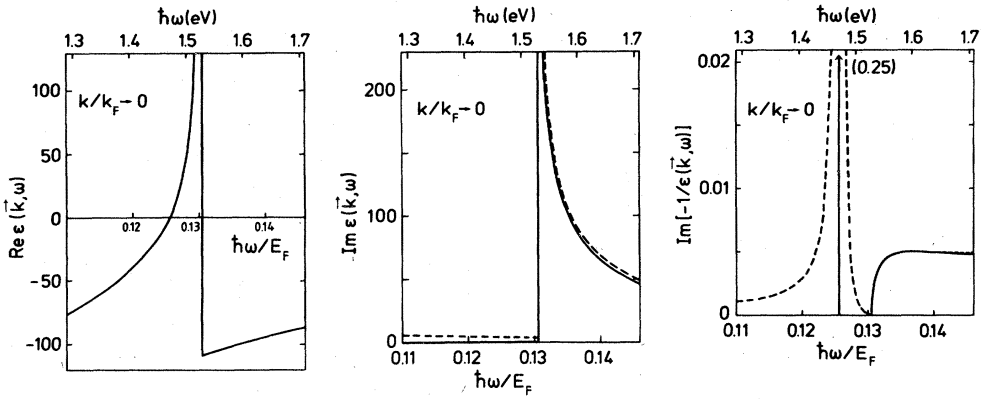

FIG. 4. $\mathrm{Im}\epsilon_M(\vec{k},\omega)$, $\mathrm{Re}\epsilon_M(\vec{k},\omega)$ and $\mathrm{Im}[-1/\epsilon_M(\vec{k},\omega)]$ for $\vec{k}\to\vec{0}$. Theoretical results with (dashed line) and without (solid line) the inclusion of the effect of the pseudopotential form factor $V_{111}\neq 0$ are compared. Notice that results for $\mathrm{Re}\epsilon_M(\vec{0},\omega)$ are essentially the same. The number in parenthesis for $\mathrm{Im}[-1/\epsilon_M(\vec{0},\omega)]$ indicates the height of the loss function at the peak position.

The total absorption is obtained by adding the intraband term which, in absence of any disorder scattering, is highly singular at $\omega=0$ and zero otherwise. Scattering due to phonons and other lattice defects gives rise to what is usually accounted for by the Drude absorption in the relaxation time τ approximation properly modified by the optical mass instead of the free-electron mass to satisfy the conductivity sum rule. There is another peak[9] to be expected near $\omega=2|V_{111}|$. Since $|V_{111}|\approx\frac{1}{3}|V_{200}|$ it occurs at a smaller energy, where it is concealed in the Drude term as shown by experiment. Its contribution to $\mathrm{Im}\epsilon_M(\vec{k}\to\vec{0},\omega)=4\pi\,\mathrm{Re}\sigma(\omega)/\omega$ near $\omega=2|V_{200}|$ is very small, as shown in Fig. 4(b).

For $\omega\gg 2|V_G|$ one observes that $\mathrm{Im}\epsilon_M(\vec{k}\to\vec{0},\omega)$ reduces to

$$\mathrm{Im}\epsilon_M(\vec{k}\to\vec{0},\omega)=\tfrac{4}{3}\sum_{\vec{G}}\frac{|V_G|^2G^4}{\omega^4}\mathrm{Im}\epsilon_L(G,\omega)\,, \qquad (2.3)$$

which is the result obtained in nondegenerate perturbation theory.[2] This provides the first argument against the objections of Möller and Otto,[12] Bross,[18] and Gibbons[19] against the use of nondegenerate perturbation theory for $\omega\sim\omega_p$. We shall demonstrate that the same is true at finite $k\leq k_c$.

From $\mathrm{Im}\epsilon_M(\vec{k}\to\vec{0},\omega)$ with the proper inclusion of the intraband term, it is straightforward to derive $\mathrm{Re}\epsilon_M(\vec{k}\to\vec{0},\omega)$ by application of the Kramers-Kronig relations and the sum rule. Neglecting scattering effects ($\tau\to\infty$) this leads to

$$\mathrm{Re}\epsilon(\vec{k}\to\vec{0},\omega)=1-\frac{\omega_p^2}{\omega^2}+\tfrac{4}{3}\sum_{\vec{G}}\frac{|V_G|^2G^4}{\omega^4}I(G,\omega)\,, \qquad (2.4)$$

where

$$I(G,\omega)=\frac{1}{\pi}\int_{2|V_G|}^{\infty}d\omega'\left[\frac{1}{\omega'-\omega}+\frac{1}{\omega'+\omega}-\frac{2}{\omega'}\right]\times\frac{\mathrm{Im}\tilde{\epsilon}_L(G,\omega')}{[1-(2V_G/\omega')^2]^{1/2}}\,.$$

The integral can be expressed in terms of elementary functions as outlined in Appendix A. We are now able to calculate the loss function $\mathrm{Im}[-1/\epsilon_M(\vec{k}\to\vec{0},\omega)]$. In Fig. 4, $\epsilon_M(\vec{k}\to\vec{0},\omega)$ and the loss function are shown for $\omega\approx 2|V_{200}|$ with and without the inclusion of the effect of V_{111}. One observes that the strong interband transitions that give rise to the square-root singularity in $\mathrm{Im}\epsilon_M(\vec{k}\to\vec{0},\omega)$ cause another zero in $\mathrm{Re}\epsilon_M(\vec{k}\to\vec{0},\omega)$ at an energy slightly below $\omega=2|V_{200}|$ and hence another pole in the loss function at this energy as was observed by Boersch *et al.*[4] many years ago. Although the difference in the positions of the peaks of $\mathrm{Im}\epsilon_M(\vec{k}\to\vec{0},\omega)$ and of $\mathrm{Im}[-1/\epsilon_M(\vec{k}\to\vec{0},\omega)]$ is very small, it is important to note.

If the effect of V_{111} is taken into account, the loss function exhibits an antinode at $\omega=2|V_{200}|$ and its asymmetric line shape is reminiscent of a Breit-Wigner or Fano[20] resonance. It arises from the Coulomb interaction of the new sharp collective mode associated with the strong interband polarization near $|2V_{200}|$ and the background of interband transitions resulting from the tail of the transitions near the (111) zone planes. If the effect of V_{111} is neglected, the loss function becomes a δ function at the energy of the new collective mode.

We should point out here that although we are specifically concerned with Al, a large number of polyvalent simple metals such as Mg, Zn, Cd, In, and Sn, for example, exhibit a similar structure in their optical properties, noticeable as a dip in the reflectivity at an energy of the order of the band gap. Its origins are precisely the strong interband transitions between single-particle states at the zone boundary. Thus Al serves as a typical example of studying the dielectric properties of a group of polyvalent simple metals and due to some peculiarities it is particularly suited for this purpose as will be discussed below.

It is worth mentioning that although the monovalent alkali metals do not exhibit such a singular behavior in their optical properties, the collective mode whose k dependence in Al we are going to study in some detail should exist for k larger than some critical value as can be understood from the work of Foo and Hopfield.[3]

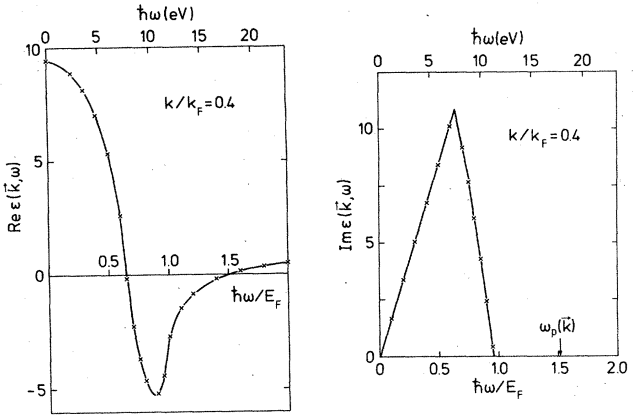

FIG. 5. Comparison between the Lindhard $\mathrm{Re}\epsilon_L(k,\omega)$ and $\mathrm{Im}\epsilon_L(k,\omega)$ (crosses) and $\mathrm{Re}\epsilon_M(\vec{k},\omega)$ and $\mathrm{Im}\epsilon_M(\vec{k},\omega)$ (full lines) for $\vec{k}$ parallel to the [100] direction obtained by considering the influence of Bragg reflection of electrons from just one Bragg plane defined by a $\vec{G}$ vector perpendicular to $\vec{k}$.

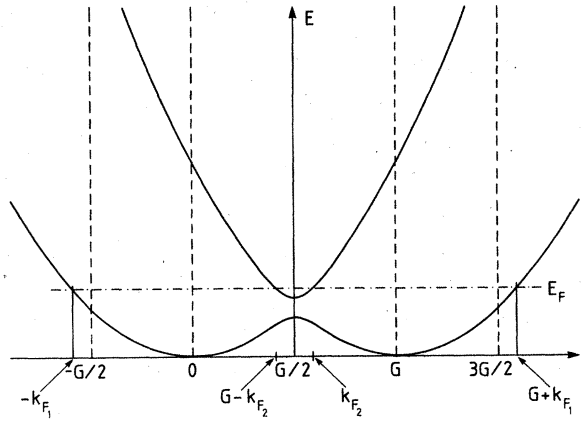

FIG. 6. Two-band model (schematically).

We now list and discuss the assumptions that go into our model calculation of $\epsilon_M(\vec{k},\omega)$ for $\vec{k}\neq\vec{0}$ from which the results shown in Figs. 1 and 2 are derived.

(i) Local field effects are fairly small in most simple metals[2] and we assume (as for $\vec{k}\to\vec{0}$)

$$\epsilon_M(\vec{k},\omega)=1/\epsilon^{-1}_{\vec{0}\,\vec{0}}(\vec{k},\omega)\approx\epsilon_{\vec{0}\,\vec{0}}(\vec{k},\omega)\ ,$$

where $\{\epsilon^{-1}_{\vec{G}\,\vec{G}'}(\vec{k},\omega)\}$ is the inverse of the dielectric matrix $\{\epsilon_{\vec{G}\,\vec{G}'}(\vec{k},\omega)\}$.

(ii) In Al a sufficiently accurate band structure in the neighborhood of the Fermi level involves only the V_{200} and V_{111} pseudopotential form factors. Since $|V_{111}|\ll E_F$ and $|V_{200}|\ll E_F$ perturbation theory can be applied. Since $|V_{111}|^2\approx 0.1\,|V_{200}|^2$ we neglect the effect of V_{111}. This appreciably simplifies our calculation and enables us to carry out most of the calculation analytically. The main reason for this is the following observation.

(iii) There are six equivalent G_{200} reciprocal-lattice vectors which can be thought to be parallel to one axis of a Cartesian coordinate system. In accordance with experiment we consider the case $\vec{k}$ parallel to $\vec{G}_{200}$ (and antiparallel to $\vec{G}_{\bar{2}00}$). Then $\vec{k}$ is perpendicular to the remaining four $\vec{G}$ vectors of the set, i.e., $\vec{G}_{020}$, $\vec{G}_{0\bar{2}0}$, $\vec{G}_{002}$, $\vec{G}_{00\bar{2}}$. The Bragg reflection of the conduction electrons from those Bragg planes defined by the four $\vec{G}$ vectors perpendicular to $\vec{k}$ has very little effect on the dielectric function. A study of the influence of just one Bragg plane with $\vec{G}\perp\vec{k}$ reveals that the resulting dielectric function is practically identical with the Lindhard function (see Fig. 5). Further reasons for this behavior are given below.

To calculate $\epsilon_M(\vec{k},\omega)$ we arrive at a model band structure that is modified from the free-electron band structure by two Bragg planes defined by $\vec{G}_{200}$ and $\vec{G}_{\bar{2}00}$. Figure 6 illustrates the model band structure. Using this band structure to calculate $\epsilon_M(\vec{k}\to\vec{0},\omega)$, one immediately recovers the result of Ashcroft and Sturm with only $V_{200}\neq 0$. Interband transitions for ω of the order of the energy gap $E_{\mathrm{gap}}=|2V_{200}|$ are treated rather accurately in this way whereas for $\omega>E_{\mathrm{gap}}$ the resulting $\epsilon_M(\vec{k}\to\vec{0},\omega)$ goes over into the result obtained by nondegenerate perturbation theory.

It is clear that our model calculation is less accurate than the rather extensive numerical calculation by Singhal.[8] In particular, we neglect the effect of interband transitions associated with higher Fourier coefficients of the pseudopotential. These interband transitions take place at higher energies and therefore tend to shift the pole of the ZBCS to lower energies (see Fig. 2).

The energy bands and the appropriate single-particle eigenstates are derived from the variational ansatz

$$\psi_{\vec{p}}(\vec{r})=a_{\vec{0}}(\vec{p})e^{i\vec{p}\cdot\vec{r}}+a_{\vec{G}}(\vec{p})e^{i(\vec{p}-\vec{G})\cdot\vec{r}} \tag{2.5}$$

by diagonalizing the 2×2 matrix

$$\begin{bmatrix}\vec{p}^{\,2}-E & V\\ V & (\vec{p}-\vec{G})^2-E\end{bmatrix}, \tag{2.6}$$

where $V\equiv V_{200}>0$. We obtain

$$\left.\begin{matrix}E_1(\vec{p})\\ E_2(\vec{p})\end{matrix}\right\}=\tfrac{1}{2}[\vec{p}^{\,2}+(\vec{p}-\vec{G})^2]$$
$$\mp\tfrac{1}{2}\{[(\vec{p}-\vec{G})^2-\vec{p}^{\,2}]^2+4|V|^2\}^{1/2}\ . \tag{2.7}$$

For $\vec{p}+\vec{k}$ we introduce

$$\gamma(p_{\parallel},\vec{k})=\frac{1}{2V}[(\vec{p}+\vec{k}-\vec{G})^2-(\vec{p}+\vec{k})^2]$$
$$=\frac{1}{2V}(\vec{G}^2-2p_{\parallel}G-2\vec{k}\cdot\vec{G})\ . \tag{2.8}$$

We decompose $\vec{p}=(\vec{p}_{\parallel},\vec{p}_{\perp})$ with $p_{\parallel}=\vec{p}\cdot\vec{G}/G$ and $\vec{p}_{\perp}\cdot\vec{G}=0$ and have

$$\left.\begin{matrix} E_1(\vec{p}+\vec{k}) \\ E_2(\vec{p}+\vec{k}) \end{matrix}\right\} = p_\perp^2 + \frac{G^2}{4} + \frac{V^2}{G^2}\gamma^2(p_{||},\vec{k}) \mp V[\gamma^2(p_{||},\vec{k})+1]^{1/2} \tag{2.7'}$$

and

$$\left.\begin{matrix} [a_{\vec{0}}(\vec{p}+\vec{k})]_1 \\ [a_{\vec{0}}(\vec{p}+\vec{k})]_2 \end{matrix}\right\} = \mp\frac{1}{\sqrt{2}}\left[1 \pm \frac{\gamma(p_{||},\vec{k})}{[\gamma^2(p_{||},\vec{k})+1]^{1/2}}\right]^{1/2}, \tag{2.9}$$

$$\left.\begin{matrix} [a_{\vec{G}}(\vec{p}+\vec{k})]_1 \\ [a_{\vec{G}}(\vec{p}+\vec{k})]_2 \end{matrix}\right\} = \frac{1}{\sqrt{2}}\left[1 \mp \frac{\gamma(p_{||},\vec{k})}{[\gamma^2(p_{||},\vec{k})+1]^{1/2}}\right]^{1/2}.$$

Then $\psi_{1\vec{p}}(\vec{r})$ and $\psi_{2\vec{p}}(\vec{r})$ are orthogonal and normalized.

We now evaluate $\epsilon_M(\vec{k},\omega) \approx \epsilon_{\vec{0}\,\vec{0}}(\vec{k},\omega)$ within the two-band model. In general we have

$$\epsilon_{\vec{0}\,\vec{0}}(\vec{k},\omega) = 1 - \frac{4\pi e^2}{k^2}\left[2\sum_{\vec{k}}\sum_{l,l'=1}^{2}\frac{f(E_l(\vec{p}))-f(E_{l'}(\vec{p}+\vec{k}))}{\omega+i\delta+E_l(\vec{p})-E_{l'}(\vec{p}+\vec{k})}\,|\langle l\vec{p}\,|\,e^{-i\vec{k}\cdot\vec{r}}\,|\,l',\vec{p}+\vec{k}\rangle|^2\right]$$

$$= 1 - \frac{4\pi e^2}{k^2}\left[2\sum_{\vec{p}}\sum_{l,l'=1}^{2} f(E_l(\vec{p}))\left[\frac{|\langle l\vec{p}\,|\,e^{-i\vec{k}\cdot\vec{r}}\,|\,l',\vec{p}+\vec{k}\rangle|^2}{\omega+i\delta+E_l(\vec{p})-E_{l'}(\vec{p}+\vec{k})} - \frac{|\langle l',\vec{p}-\vec{k}\,|\,e^{-i\vec{k}\cdot\vec{r}}\,|\,l,\vec{p}\rangle|^2}{\omega+i\delta+E_{l'}(\vec{p}-\vec{k})-E_l(\vec{p})}\right]\right]. \tag{2.10}$$

For intraband transitions, i.e., $l=l'$, we find

$$M_{ll}(p_{||},\vec{k}) \equiv |\langle l\vec{p}\,|\,e^{-i\vec{k}\cdot\vec{r}}\,|\,l,\vec{p}+\vec{k}\rangle|^2 = \frac{1}{2}\left[1+\frac{\gamma(p_{||},\vec{0})\gamma(p_{||},\vec{k})+1}{[\gamma^2(p_{||},\vec{0})+1]^{1/2}[\gamma^2(p_{||},\vec{k})+1]^{1/2}}\right]. \tag{2.11}$$

For interband transitions, i.e., $l\neq l'$, we find

$$M_{ll'}(p_{||},\vec{k}) \equiv |\langle l\vec{p}\,|\,e^{-i\vec{k}\cdot\vec{r}}\,|\,l',\vec{p}+\vec{k}\rangle|^2 = \frac{1}{2}\left[1-\frac{\gamma(p_{||},\vec{0})\gamma(p_{||},\vec{k})+1}{[\gamma^2(p_{||},\vec{0})+1]^{1/2}[\gamma^2(p_{||},\vec{k})+1]^{1/2}}\right]. \tag{2.12}$$

Note, if $\vec{k}$ is perpendicular to $\vec{G}$, then $\gamma(p_{||},\vec{k})=\gamma(p_{||},\vec{0})$ and consequently $M_{ll}(p_{||},\vec{k})=1$ and $M_{ll'}=0$ for $l\neq l'$. Only intraband transitions can occur in this case. The energy difference is given by

$$E_l(\vec{p}+\vec{k})-E_l(\vec{p}) = k^2+2\vec{k}\cdot\vec{p}$$

and thus for $\vec{k}\perp\vec{G}$ we obtain

$$\epsilon_{00}(\vec{k},\omega) = 1 - \frac{4\pi e^2}{k^2}\left[2\sum_{\vec{p}}[f(E_1(\vec{p}))+f(E_2(\vec{p}))]\left[\frac{1}{\omega+i\delta-2\vec{p}\cdot\vec{k}-k^2} - \frac{1}{\omega+i\delta-2\vec{p}\cdot\vec{k}+k^2}\right]\right]. \tag{2.13}$$

The close similarity to the Lindhard function is obvious from (2.13). The numerical evaluation confirms it to the point that for all practical applications it is indistinguishable from the Lindhard function (see Fig. 5). This proves that the influence of those Bragg planes with $\vec{G}\perp\vec{k}$ on the response function is negligible. Details of the integration of (2.13) are outlined in Appendix B.

We now proceed to calculate the dielectric function $\epsilon_{\vec{0}\,\vec{0}}(\vec{k},\omega)$ for $\vec{k}$ parallel to $\vec{G}_{200}$ (and antiparallel to $\vec{G}_{\bar{2}00}$) neglecting the effect of the Bragg planes defined by $\vec{G}$ vectors perpendicular to $\vec{k}$ altogether. $\epsilon_{\vec{0}\,\vec{0}}(\vec{k},\omega)$ is easily evaluated because neither the matrix elements $M_{ll'}(p_{||},\vec{k})$ nor the energy differences depend on $p_\perp$ and φ, and the $\vec{p}$ integral is conveniently evaluated using cylindrical coordinates. We introduce the following notation

$$\omega_{ll'}(p_{||},\vec{k}',\vec{k}) = E_{l'}(\vec{p}+\vec{k})-E_l(\vec{p}+\vec{k}'), \tag{2.14}$$

$$\left.\begin{matrix}[p_1^2(p_{||})]_{1,\max}\\ [p_1^2(p_{||})]_{2,\max}\end{matrix}\right\}=E_F-\frac{G^2}{4}-\frac{V^2}{G^2}\gamma^2(p_{||},\vec{0})\pm V[\gamma^2(p_{||},\vec{0})+1]^{1/2}\,, \tag{2.15}$$

and the 2×2 matrices

$$p_1=\begin{bmatrix}0 & -k_{F_1}\\ G-k_{F_2} & G-k_{F_2}\end{bmatrix}, \tag{2.16}$$

$$p_2=\begin{bmatrix}G & G+k_{F_1}\\ k_{F_2} & k_{F_2}\end{bmatrix}, \tag{2.17}$$

and obtain

$$\mathrm{Re}\epsilon_{\vec{0}\,\vec{0}}(\vec{k},\omega)=1-\frac{3\omega_p^2}{8k^2}\sum_{l,l'=1}^{2}\left[\int_{p_{1,II'}}^{p_{2,II'}}dp_{||}[p_1^2(p_{||})]_{l,\max}\frac{M_{II'}(p_{||},\vec{k})}{\omega-\omega_{II'}(p_{||},\vec{0},\vec{k})}-\int_{p_{1,I'I}}^{p_{2,I'I}}dp_{||}[p_1^2(p_{||})]_{l',\max}\frac{M_{II'}(p_{||},-\vec{k})}{\omega-\omega_{II'}(p_{||},-\vec{k},\vec{0})}\right] \tag{2.18}$$

and

$$\mathrm{Im}\epsilon_{\vec{0}\,\vec{0}}(\vec{k},\omega)=\frac{3\pi\omega_p^2}{8k^2}\sum_{l,l'=1}^{2}\left[\sum_{p_1(\vec{k},\omega)}\left[[p_1^2(p_{||})]_{l,\max}M_{II'}(p_{||},\vec{k})\left|\frac{\partial\omega_{II'}(p_{||},\vec{0},\vec{k})}{\partial p_{||}}\right|^{-1}\right]_{p_{||}=p_1(\vec{k},\omega)}\right.$$
$$\left.-\sum_{p_2(\vec{k},\omega)}\left[[p_1^2(p_{||})]_{l',\max}M_{II'}(p_{||},-\vec{k})\left|\frac{\partial\omega_{II'}(p_{||},-\vec{k},0)}{\partial p_{||}}\right|^{-1}\right]_{p_{||}=p_2(\vec{k},\omega)}\right], \tag{2.19}$$

where $p_1(\vec{k},\omega)$ are solutions of

$$\omega=\omega_{II'}(p_1,\vec{0},\vec{k}),\quad \text{with } (p_1)_{II'}<p_1<(p_2)_{II'}\,, \tag{2.20}$$

and $p_2(\vec{k},\omega)$ are solutions of

$$\omega=\omega_{II'}(p_2,-\vec{k},0),\quad \text{with } (p_1)_{I'I}<p_2<(p_2)_{I'I}\,. \tag{2.21}$$

$p_1(\vec{k},\omega)$ and $p_2(\vec{k},\omega)$ are found numerically and the $p_{||}$ integration of the principal-value integral in (2.18) is carried out numerically.

The equations (2.18) and (2.19) are our main results and form the basis of the discussion in the next section.

III. RESULTS AND DISCUSSIONS

To discuss the characteristic changes in $\epsilon_M(\vec{k},\omega)$ induced by the Bragg reflection of the conduction electrons from the two Bragg planes in Figs. 7, 8, and 9, $\mathrm{Im}\epsilon_M(\vec{k},\omega)$, $\mathrm{Re}\epsilon_M(\vec{k},\omega)$, and $\mathrm{Im}[-1/\epsilon_M(\vec{k},\omega)]$ are plotted for three different $\vec{k}$ values along the [100] direction and compared with their free-electron counterparts $\mathrm{Im}\epsilon_L(k,\omega)$, $\mathrm{Re}\epsilon_L(k,\omega)$, and $\mathrm{Im}[-1/\epsilon_L(k,\omega)]$. We observe that due to the gap in the band structure a gap is also created in the single-particle excitation spectrum (Fig. 7). The oscillator strength that is missing inside the gap is

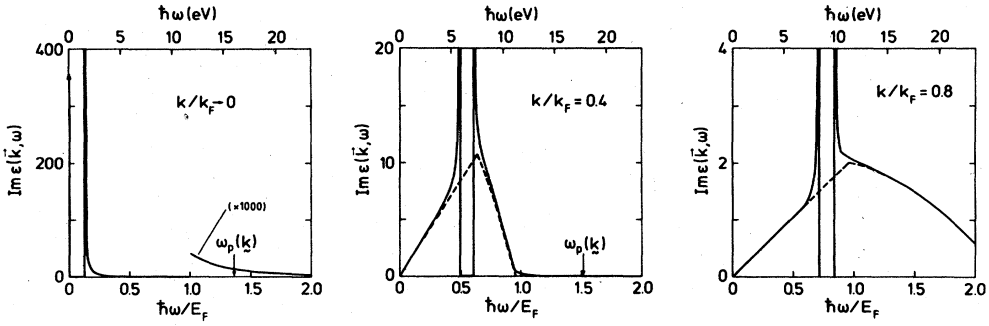

FIG. 7. $\mathrm{Im}\epsilon_M(\vec{k},\omega)$ for three different values of $\vec{k}$ along the [100] direction within the first Brillouin zone as functions of ω. Solid line: present theory; dashed lines: Lindhard $\mathrm{Im}\epsilon_L(k,\omega)$. Arrow for $k\to0$ at $\omega=0$ indicates singular behavior of $\mathrm{Im}\epsilon_L(k,\omega)$. Notice different scales on vertical axes.

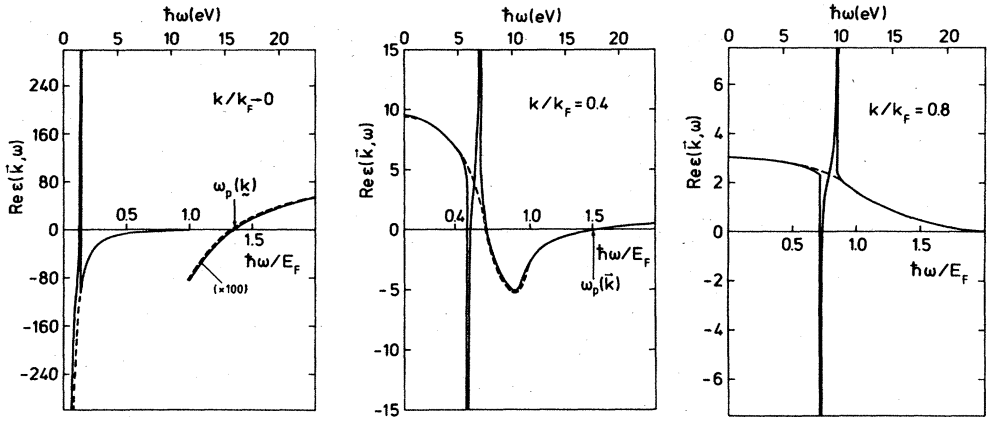

FIG. 8. $\mathrm{Re}\epsilon_M(\vec{k},\omega)$ for three different values of $\vec{k}$ along the [100] direction within the first Brillouin zone as functions of ω. Solid line: present theory; dashed line: Lindhard $\mathrm{Re}\epsilon_L(k,\omega)$. Notice different scales on vertical axes.

shifted into van Hove singularities[21] of the joint density of states (JDOS) at the edges of the gap. The resonancelike structures in the single-particle excitation spectrum cause an oscillation in $\mathrm{Re}\epsilon_M(\vec{k},\omega)$ (Fig. 8) with the consequence of another zero in $\mathrm{Re}\epsilon_M(\vec{k},\omega)$ for ω inside this gap, and hence an additional pole in the loss function (Fig. 9): A new collective mode exists.

In general, a singular structure in the JDOS can occur at some energy ω, when

$$\omega=\omega_{ll'}(\vec{p},\vec{k})=E_{l'}(\vec{p}+\vec{k})-E_l(\vec{p}) \tag{3.1}$$

and

$$\vec{\nabla}_{\vec{p}}\omega_{ll'}(\vec{p},\vec{k})=\vec{\nabla}_{\vec{p}}[E_{l'}(\vec{p}+\vec{k})-E_l(\vec{p})]=0\,, \tag{3.2}$$

or, equivalently,

$$\vec{\nabla}_{\vec{p}}E_{l'}(\vec{p}+\vec{k})=\vec{\nabla}_{\vec{p}}E_l(\vec{p})\,. \tag{3.2'}$$

Within our present model $\omega_{ll'}(\vec{p},\vec{k})$ depends on $p_{||}$ only, and (3.2) reduces to $\partial\omega_{ll'}(p_{||},k)/\partial p_{||}=0$. Since the matrix elements, also depend on $p_{||}$, only the singular structure is not integrated out by the $\vec{p}_\perp$ integration; there are various ways to illustrate the origin of the effect in our present model. In Fig. 10(a), intraband and interband excitations are plotted as functions of $p_{||}$ for a fixed $\vec{k}$. They are separated by a gap and show a maximum of $\omega_{11}(p_{||},\vec{k})$ at $p_{||,1}$ and a minimum of $\omega_{12}(p_{||},\vec{k})$ at $p_{||,2}$, i.e., Eq. (3.2) is satisfied. In Fig. 10(b) the origin of the effect is traced back to the property of the band structure itself. Points (i.e., planes in $\vec{p}$ space) defined by $p_{||}=p_{||,1}$ and $p_{||}=p_{||,2}$ for which (3.2') is satisfied are exhibited. Note that both for intraband and interband transitions the final states are close to the (200) zone boundary, hence the name "zone-boundary collective state." Equations (3.1) and (3.2) can be used to eliminate $p_{||,1}$ and $p_{||,2}$, and the resulting curves $\omega_{11}(\vec{k})$ and $\omega_{12}(\vec{k})$ are the loci of the points $(\vec{k},\omega)$ for $\vec{k}||[100]$ for which $\mathrm{Im}\epsilon_M(\vec{k},\omega)$ is singular. In other words, $\omega_{11}(\vec{k})$ and $\omega_{12}(\vec{k})$ define the gap and enclose the dispersion of the new collective mode (see Fig. 11). $\omega_{11}(\vec{k})$ and $\omega_{12}(\vec{k})$ must be determined numerically, however, and one can obtain approximate formulas for sufficiently large k (for $k>0.1$) because then the initial state is sufficiently far away from the zone boundary and its energy can be replaced by the unperturbed free-electron energy. We obtain, for $\vec{k}||[100]$,

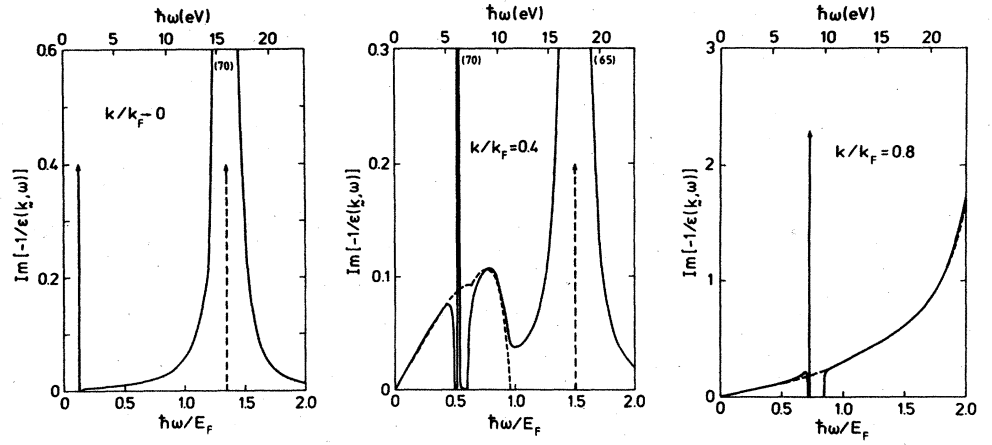

FIG. 9. $\mathrm{Im}[-1/\epsilon_M(\vec{k},\omega)]$ for three different values of $\vec{k}$ along the [100] direction within the first Brillouin zone as functions of ω. Solid line: present theory; dashed line: Lindhard $\mathrm{Im}[-1/\epsilon_L(k,\omega)]$. Arrows indicate the δ functions. Notice different scales on vertical axes.

$$\omega_{11,2}(\vec{k}) \approx k(G-k) \mp \frac{V}{2}\left[\left[\frac{(G-2k)^2}{k(G-k)}+4\right]^{1/2} - \frac{(G-2k)^2}{G\sqrt{k(G-k)}}\right]$$

$$\approx k(G-k) \mp V\left[1-\tfrac{1}{2}\frac{(G-2k)^2}{\sqrt{k(G-k)}}\left[\frac{1}{G}-\frac{1}{4\sqrt{k(G-k)}}\right]\right]. \tag{3.3}$$

Within the same approximation the width of the gap in the single-particle spectrum $\Delta\omega(\vec{k})$ follows from (3.3),

$$\Delta\omega(k) = \omega_{12}(k) - \omega_{11}(k) \approx V\left[\left[\frac{(G-2k)^2}{k(G-k)}+4\right]^{1/2} - \frac{(G-2k)^2}{G\sqrt{k(G-k)}}\right]$$

$$\approx 2V\left[1-\tfrac{1}{2}\frac{(G-2k)^2}{\sqrt{k(G-k)}}\left[\frac{1}{G}-\frac{1}{4\sqrt{k(G-k)}}\right]\right]. \tag{3.4}$$

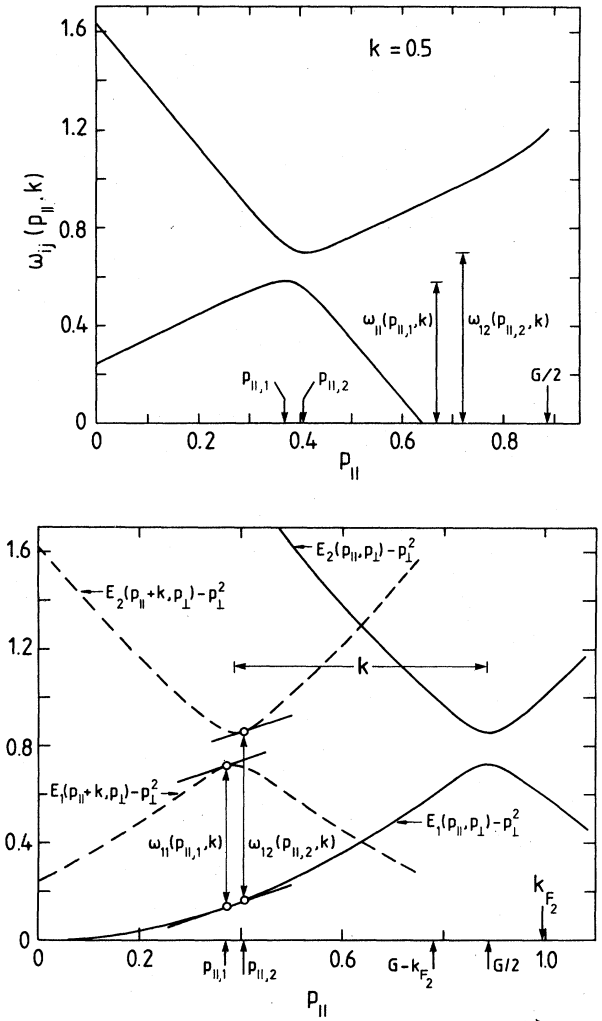

FIG. 10. (a) Intraband excitation energy $\omega_{11}(p_{||},\vec{k})$ within first band (lower curve) and interband excitation energy $\omega_{12}(p_{||},\vec{k})$ from band 1 to band 2 (upper curve) for $k/k_F=0.5$ as a function of $p_{||}$. (b) Model band structure along the [100] direction (full curves). Dashed curves correspond to the model band structure shifted by $k/k_F=0.5$, i.e., a "direct" transition from the lower band (band 1) to one of the dashed bands corresponds to an indirect transition from $p_{||}$ (band 1) to $p_{||}+k$ (band 1 or 2).

Note that crudely speaking the position of the gap is given by $\omega \approx k(G-k)$ for $\vec{k}||[100]$, a result previously obtained by Foo and Hopfield.[3] This formula can also be used as a rough estimate of the dispersion of the collective mode. It is directly obvious from the band structure that $\Delta\omega(\vec{k}\to 0)=2V$. From (3.4) it follows that $\Delta\omega(\vec{G}/2)=2V$, whereas for intermediate $\vec{k}$ values, $\Delta\omega(\vec{k})<2V$. Note also that the gap $\Delta\omega(\vec{k})$ is not absolute in some k regime bounded in Fig. 11 by two parallel lines. For these $\vec{k}$ values there are intraband transitions $\omega_{22}(p_{||},\vec{k})$ within the second band. Since the occupancy of the second band is very small, the contribution of these $\vec{k}$ values to $\mathrm{Im}\epsilon_M(\vec{k},\omega)$ is extremely weak. Where this regime overlaps the dispersion of the new collective mode, it leads to a small finite linewidth (see Fig. 9: $k/k_F=0.4$), whereas outside this k regime the collective mode is undamped within our model (see Fig. 9: $k/k_F=0$ and 0.8). For very small k, the collective mode exhibits a quadratic dispersion, as expected for symmetry reasons (Fig. 12).

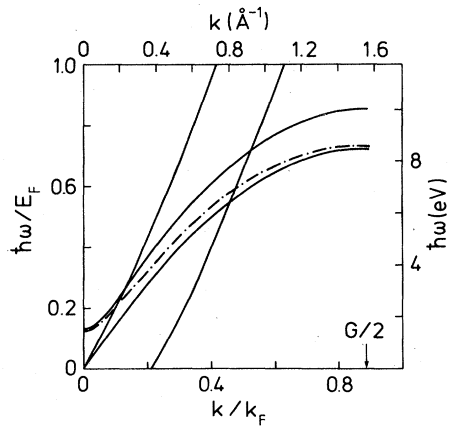

FIG. 11. Dispersion of the (200) ZBCS (dash-dotted line). The two solid lines which enclose the dispersion of the ZBCS indicate the borderline of the gap in the single-particle excitation spectrum of the present theory and are associated with van Hove singularities in the joint density of states and with singularities in $\mathrm{Im}\epsilon_M(\vec{k},\omega)$. The two parallel solid lines define the (k,ω) regime where intraband transitions $\omega_{22}(p_{||},\vec{k})$ within the second band occur.

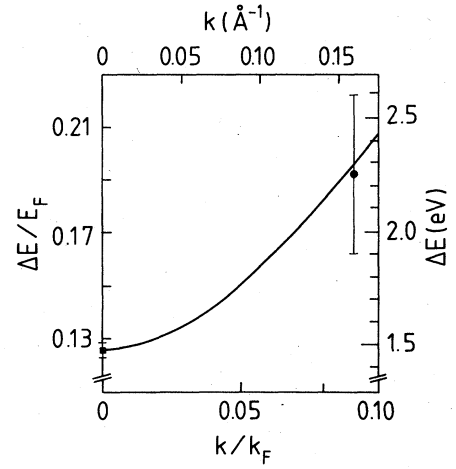

FIG. 12. Dispersion of the (200) ZBCS for small values of k. Experimental EELS data are from Chen and Silcox (Ref. 7) (solid circle) and Boersch *et al.* (Ref. 4) (solid square).

In the monovalent alkali metals, the mode cannot exist for small k, because there are no occupied states near the zone boundary. The minimum k can be estimated roughly from the crossing of the border lines of the free-electron single-particle excitation spectrum $\omega=k^2+2k$ and of the estimate of the position of the gap $\omega=k(G_{110}-k)$. One finds $k_{\min}=G_{110}/2-1=0.14$ and $\omega=G_{110}^2/4-1$ as an estimate for the corresponding energy of the mode at $k_{\min}$.

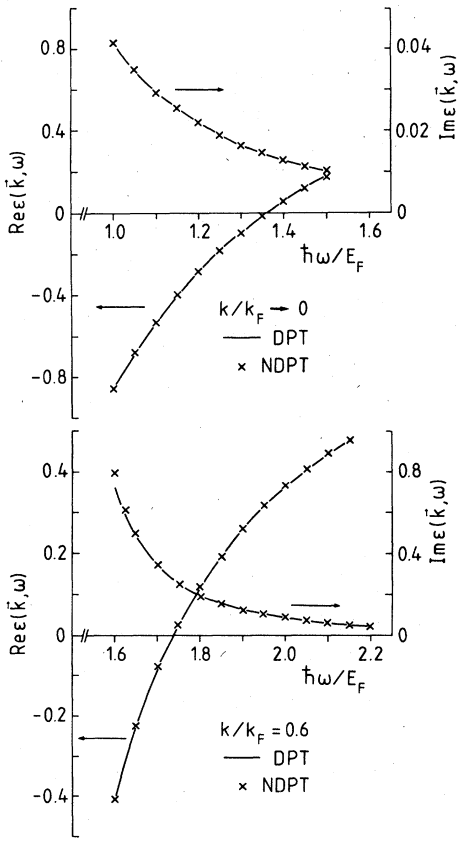

FIG. 13. Comparison of results in the high-frequency regime ($\omega \gg |2V|$) for $\mathrm{Re}\epsilon_M(\vec{k},\omega)$ and $\mathrm{Im}\epsilon_M(\vec{k},\omega)$ for $\vec{k}\to\vec{0}$ and $k/k_F=0.6$ along the [100] direction, evaluated in degenerate (full curves) and nondegenerate (crosses) perturbation theory. Notice different scales on vertical axes.

Returning to polyvalent aluminum, in reality broadening of the ZBCS occurs due to disorder scattering and interband transitions associated with the V_{111} pseudopotential form factor, whose effect is neglected in our model. However, as can be observed from the loss function for $\vec{k}\to\vec{0}$, the peak in the loss function is still very sharp even when the effect of V_{111} is included. This also remains true when disorder effects via a constant relaxation time are taken into account. Hence we can expect on theoretical grounds that the collective mode is well defined throughout the zone, as is borne out experimentally.

A more essential reason that this mode is observable in EELS even for large $\vec{k}$ is the increase of the strength of the mode with increasing $\vec{k}$, as shown in Fig. 3. The discrepancy between theory and experiment at large k is very likely to be due to the overlap with the loss spectrum centered at the (200) elastic scattering point in k space. The $\vec{k}$ dependence of the strength is a characteristic feature of this collective mode, in comparison with the monotonically decreasing strength of the plasmon with increasing k, shown by a dashed curve in Fig. 3. Note, however, that the overall strength of the ZBCS is 2 orders of magnitude smaller than the overall strength of the plasmon. A rough estimate of the order of magnitude can be derived from a simple sum-rule argument,

$$\int_{\omega_{11}(\vec{k})}^{\omega_{12}(\vec{k})} d\omega\,\omega\,\mathrm{Im}\left[\frac{-1}{\epsilon_L(k,\omega)}\right] \approx \int_{\omega_{11}(\vec{k})}^{\omega_{12}(\vec{k})} d\omega\,\omega\pi\,\delta(\omega-\omega_{\mathrm{ZBCS}}(\vec{k}))\left|\frac{\partial\,\mathrm{Re}\epsilon_M(k,\omega)}{\partial\omega}\right|^{-1}. \tag{3.5}$$

It follows from (3.5) that

$$\pi\left|\frac{\partial\,\mathrm{Re}\epsilon_M(\vec{k},\omega)}{\partial\omega}\right|^{-1}_{\omega=\omega_{\mathrm{ZBCS}}(\vec{k})} \approx \Delta\omega(\vec{k})\,\mathrm{Im}\left[\frac{-1}{\epsilon_L(k,\omega_{\mathrm{ZBCS}}(\vec{k}))}\right], \tag{3.6}$$

where $\Delta\omega(\vec{k})$ is the width of the gap defined by (3.4). Since $\Delta\omega(\vec{k})$ is proportional to V, the strength of the mode is essentially proportional to V.

Finally, we apply our theory to the plasmon in order to discuss the influence of interband transitions associated, in particular, with V_{200} on the small-k plasmon dispersion. The purpose is to clarify the controversy between the work of Möller and Otto,[12] and Sturm.[13] In Figs. 13(a) and 13(b) results for $\epsilon_M(\vec{k},\omega)$ for $\vec{k}\to\vec{0}$ and $k=0.6$ evaluated in degenerate and nondegenerate perturbation theory are compared for ω near $\omega_p(k)$. The results are practically indistinguishable. Consequently, the plasmon dispersion is the same in both approximations [see Fig. 14(a)]. Thus the discrepancy in the small-k quadratic dispersion constant α, defined by

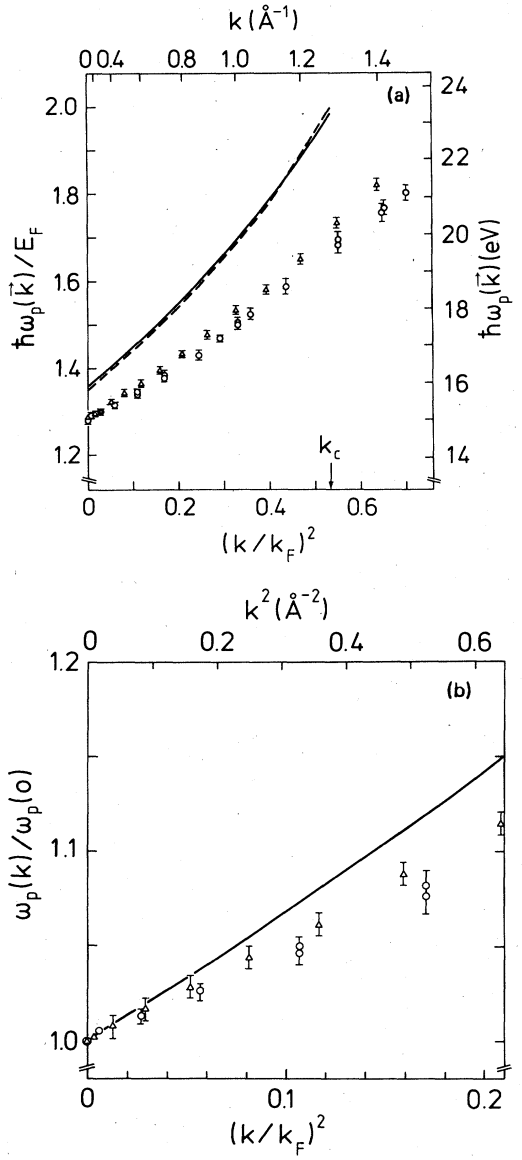

FIG. 14. (a) Plasmon dispersion in Al: comparison between theory and experiment. Full line: degenerate and nondegenerate perturbation theory along [100] direction; dashed line: obtained from $\epsilon_L(k,\omega)$. (b) Reduced plasmon dispersion $\omega_p(k)/\omega_p(0)$ in the small-k regime. Full line: present theory along [100] direction. Experimental EELS data in (a) and (b) are from Urner-Wille and Raether (Ref. 22) ([100] direction, triangles) and Petri and Otto (Ref. 5) (polycrystalline aluminum, open circles).

$$\omega_p(k)=\omega_p(0)+2\alpha k^2+\cdots\ , \tag{3.7}$$

between its free-electron RPA estimate $\alpha_{\mathrm{RPA}}=3/(5\omega_p)$ and the value determined from EELS, is not reconciled by the inclusion of interband transitions associated with the V_{200} pseudopotential form factor. This is demonstrated by Fig. 14(b). The EELS data shown in Figs. 14(a) and 14(b) are from Urner-Wille and Raether,[22] and Petri and Otto.[5]

IV. CONCLUSIONS

In this work we have clarified the nature of a sharp structure observed in the EELS of Al for $\vec{k}$ parallel to the [100] direction throughout the first BZ. It is a collective excitation of the conduction electrons, the so-called zone-boundary collective state, brought about by the reflection of the conduction electrons from a pair of (200) Bragg planes and is therefore a true band-structure effect, in contrast to the plasmon. The situation for the (200) ZBCS in Al is ideal because there is no destructive interference from the remaining four {200} Bragg planes as discussed in Sec. II. Lifetime effects from phonon-assisted transitions and transitions associated with the V_{111} pseudopotential form factor are small in the sense that the resulting linewidth of the ZBCS is small compared with the width of the gap. This can be inferred from the $\vec{k}\to\vec{0}$ case. A similarly favorable situation should be present in polyvalent simple metals of hcp structure, such as Be, Mg, Zn, and Cd, provided $\vec{k}$ is chosen parallel to the c direction.

Although preferably one should try to observe this mode for $\vec{k}$ parallel to the $\vec{G}$ vectors that define the Bragg planes, traces of the (200) ZBCS can be observed for $\vec{k}$ along the [110] and [111] directions in the EELS of Petri and Otto.[5] However, the structure appears somewhat smeared due to interference effects. In the EELS (Refs. 5 and 7) additional structures at higher energies were observed. These peaks might be correlated with a (220) ZBCS. During the last ten years, structures in the EELS (Refs. 23–26) which seemingly appeared as a continuation of the plasmon beyond the theoretical cutoff wave vector k_c were attributed to many-body effects (exchange and correlation) in the electron gas beyond the RPA.[23,27,28] However, from rough estimates based on Eqs. (3.3) and (3.5), one might conjecture that these structures arise from ZBCS's associated with pairs of (311)

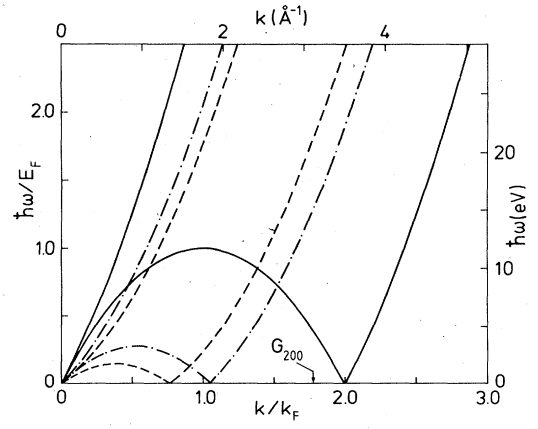

FIG. 15. Particle-hole excitation spectrum for aluminum within degenerate perturbation theory and considering the influence of Bragg reflection of electrons from just one Bragg plane defined by a $\vec{G}$ vector perpendicular to $\vec{k}$. Lines correspond, in reduced units, to $\omega=k^2+2\alpha_i k$, $\omega=k^2-2\alpha_i k$ and $\omega=2\alpha_i k-k^2$ with $\alpha_1=(E_F+V^2/G^2)^{1/2}$ (full lines), $\alpha_2=(E_F-G^2/4+V)^{1/2}$ (dot-dashed lines), and $\alpha_3=(E_F-G^2/4-V)^{1/2}$ (dashed lines).

and/or (222) Bragg planes. In this sense, very recently the anisotropy of one peak in the dynamic structure factor in Li measured by Schülke *et al.*[29] by inelastic synchrotron x-ray scattering was attributed to a ZBCS.

Quite generally, the existence of these modes will not be confined to simple metals, but can be expected to exist in more complicated systems such as the transition metals and are therefore of general interest. There is also experimental evidence for their existence in semiconductors such as Si.[30]

The above reasons for the existence of ZBCS's [see Eq. (3.2')] may be regarded as a guide to identify these modes from a given band structure. Whether they can be observed in EELS or by inelastic x-ray scattering will depend on damping effects. To identify these modes will be of great importance in the discussion of short-range correlation effects in the electron gas. The rather structureless particle-hole excitation spectrum of the homogeneous electron gas becomes structured even within the RPA due to the ZBCS's as a consequence of the periodic crystal potential (which destroys the homogeneity).

ACKNOWLEDGMENTS

One of the authors (L.E.O.) would like to acknowledge the hospitality of the Institut für Festkörperforschung der Kernforschungsanlage Jülich, where part of this work was performed, and the financial support under the Scientific Exchange Agreement between the Deutscher Akademischer Austauschdienst (DAAD) and the Brazilian National Research Council [Conselho Nacional de Desenvolvimento Cientifico e Tecnológico (CNPq)]. We are grateful to N. Schopohl for a critical reading of the manuscript.

APPENDIX A

To obtain $\mathrm{Re}\epsilon_M(k,\omega)$, Eq. (2.4), by application of the Kramers-Kronig relation from $\mathrm{Im}\epsilon_M(k,\omega)$, the following integral $I(G,\omega)$ must be evaluated:

$$I(G,\omega)=\frac{1}{\pi}\int_{2|V_G|}^{\infty}d\omega'\left[\frac{1}{\omega'-\omega}+\frac{1}{\omega'+\omega}-\frac{2}{\omega'}\right]\frac{\mathrm{Im}\tilde{\epsilon}_L(G,\omega')}{[1-(2V_G/\omega')^2]^{1/2}}\ , \tag{A1}$$

which, because of (2.2), decomposes into

$$I(G,\omega)=I_1(G,\omega)+I_2(G,\omega)\ ,$$

where

$$I_1(G,\omega)=\frac{3\omega_p^2}{16G^3}\int_{2|V_G|}^{\tilde{\omega}_1(G)}d\omega'\left[\frac{1}{\omega'-\omega}+\frac{1}{\omega'+\omega}-\frac{2}{\omega'}\right]\frac{\omega'}{[1-(2V_G/\omega')^2]^{1/2}}\ , \tag{A2}$$

and

$$I_2(G,\omega)=\frac{3}{64}\frac{\omega_p^2}{G^5}\int_{\tilde{\omega}_1(G)}^{\tilde{\omega}_2(G)}d\omega'\left[\frac{1}{\omega'-\omega}+\frac{1}{\omega'+\omega}-\frac{2}{\omega'}\right]\frac{[\tilde{\omega}_1(G)+\omega'][\tilde{\omega}_2(G)-\omega']}{[1-(2V_G/\omega')^2]^{1/2}}\ . \tag{A3}$$

All the integrals in (A2) and (A3) are standard,[31] and hence the results of the integration of (A2) and (A3) can be expressed in terms of elementary functions. We find

$$\begin{aligned}I_1(G,\omega)=&\frac{3\omega_p^2}{16G^3}\frac{\omega^2}{(\omega^2-4V_G^2)^{1/2}}\ln\left|\frac{[\tilde{\omega}_1^2(G)-4V_G^2]^{1/2}-(\omega^2-4V_G^2)^{1/2}}{[\tilde{\omega}_1^2(G)-4V_G^2]^{1/2}+(\omega^2-4V_G^2)^{1/2}}\right|\Theta(\omega-|2V_G|)\\&+\frac{3\omega_p^2}{8G^3}\frac{\omega^2}{(4V_G^2-\omega^2)^{1/2}}\arctan\left[\frac{\tilde{\omega}_1^2(G)-4V_G^2}{4V_G^2-\omega^2}\right]^{1/2}\Theta(|2V_G|-\omega)\ ,\end{aligned} \tag{A4}$$

and

$$\begin{aligned}I_2(G,\omega)=&\frac{3}{64}\frac{\omega_p^2}{G^5}\left[\frac{\omega[\tilde{\omega}_1(G)\tilde{\omega}_2(G)-\omega^2]}{(\omega^2-4V_G^2)^{1/2}}\left[\ln\left|\frac{\omega[\tilde{\omega}_2^2(G)-4V_G^2]^{1/2}-\tilde{\omega}_2(G)(\omega^2-4V_G^2)^{1/2}}{\omega[\tilde{\omega}_2^2(G)-4V_G^2]^{1/2}+\tilde{\omega}_2(G)(\omega^2-4V_G^2)^{1/2}}\right|\right.\right.\\&\left.\left.-\ln\left|\frac{\omega[\tilde{\omega}_1^2(G)-4V_G^2]^{1/2}-\tilde{\omega}_1(G)(\omega^2-4V_G^2)^{1/2}}{\omega[\tilde{\omega}_1^2(G)-4V_G^2]^{1/2}+\tilde{\omega}_1(G)(\omega^2-4V_G^2)^{1/2}}\right|\right]\\&-2\omega^2\{\mathrm{arccosh}[\tilde{\omega}_2(G)]-\mathrm{arccosh}[\tilde{\omega}_1(G)]\}\\&+\frac{\omega^2[\tilde{\omega}_2(G)-\tilde{\omega}_1(G)]}{(\omega^2-4V_G^2)^{1/2}}\left[\ln\left|\frac{[\tilde{\omega}_2^2(G)-4V_G^2]^{1/2}-(\omega^2-4V_G^2)^{1/2}}{[\tilde{\omega}_2^2(G)-4V_G^2]^{1/2}+(\omega^2-4V_G^2)^{1/2}}\right|\right.\end{aligned}$$

$$- \ln\left|\frac{[\tilde{\omega}_1^2(G)-4V_G^2]^{1/2}-(\omega^2-4V_G^2)^{1/2}}{[\tilde{\omega}_1^2(G)-4V_G^2]^{1/2}+(\omega^2-4V_G^2)^{1/2}}\right|\Bigg]\Theta(\omega-2\,|\,V_G\,|)$$

$$+\frac{3\omega_p^2}{32G^5}\left\{\frac{\omega[\tilde{\omega}_1(G)\tilde{\omega}_2(G)-\omega^2]}{(4V_G^2-\omega^2)^{1/2}}\left[\arctan\left[\frac{\omega[\tilde{\omega}_2^2(G)-4V_G^2]^{1/2}}{\tilde{\omega}_2(G)(4V_G^2-\omega^2)^{1/2}}\right]-\arctan\left[\frac{\omega[\tilde{\omega}_1^2(G)-4V_G^2]^{1/2}}{\tilde{\omega}_1(G)(4V_G^2-\omega^2)^{1/2}}\right]\right]\right.$$

$$-\omega^2\{\operatorname{arccosh}[\tilde{\omega}_2(G)]-\operatorname{arccosh}[\tilde{\omega}_1(G)]\}$$

$$\left.+\frac{\omega^2[\tilde{\omega}_2(G)-\tilde{\omega}_1(G)]}{(4V_G^2-\omega^2)^{1/2}}\left[\arctan\left[\frac{\tilde{\omega}_2^2(G)-4V_G^2}{4V_G^2-\omega^2}\right]^{1/2}-\arctan\left[\frac{\tilde{\omega}_1^2(G)-4V_G^2}{4V_G^2-\omega^2}\right]^{1/2}\right]\right\}\Theta(2\,|\,V_G\,|-\omega) \tag{A5}$$

APPENDIX B

In this Appendix, we outline the details of the integration of Eq. (2.13). We consider the influence on $\epsilon_{\vec{0}\,\vec{0}}(\vec{k},\omega)$, given by Eq. (2.13), of Bragg reflection of electrons from just one Bragg plane defined by a $\vec{G}$ vector perpendicular to $\vec{k}$. Using reduced units[14] and writing $p=(p_{\parallel},p_{\perp})$ as in the text, we have

$$\epsilon_{\vec{0}\,\vec{0}}(\vec{k},\omega)=1-\frac{3\omega_p^{02}}{8\pi k^2}\left[\int_{-k_{F_1}}^{G/2}dp_{\parallel}\int_0^{[p_{\perp}^{\max}(p_{\parallel})]_1}p_{\perp}dp_{\perp}\int_0^{2\pi}d\varphi\left[\frac{1}{\omega-k^2+i\delta-2p_{\perp}k\cos\varphi}-\frac{1}{\omega+k^2+i\delta-2p_{\perp}k\cos\varphi}\right]\right.$$

$$\left.+\int_{G/2}^{k_{F_2}}dp_{\parallel}\int_0^{[p_{\perp}^{\max}(p_{\parallel})]_2}p_{\perp}\,dp_{\perp}\int_0^{2\pi}d\varphi\left[\frac{1}{\omega-k^2+i\delta-2p_{\perp}k\cos\varphi}-\frac{1}{\omega+k^2+i\delta-2p_{\perp}k\cos\varphi}\right]\right] \tag{B1}$$

with

$$\left.\begin{matrix}[p_{\perp}^2(p_{\parallel})]_{1,\max}\\ [p_{\perp}^2(p_{\parallel})]_{2,\max}\end{matrix}\right\}=E_F-p_{\parallel}^2-\tfrac{1}{2}(G^2-2p_{\parallel}G)\pm\left[\frac{(G^2-2p_{\parallel}G)^2}{4}+V^2\right]^{1/2}, \tag{B2}$$

$$E_F=1+\frac{V^2}{4G}\ln\left|\frac{2-G}{2+G}\right|, \tag{B3}$$

$$k_{F_1}=1+\frac{V^2}{8G}\ln\left|\frac{2-G}{2+G}\right|+\frac{1}{4}\frac{V^2}{(G^2/2)+G}, \tag{B4}$$

$$k_{F_2}=1+\frac{V^2}{8G}\ln\left|\frac{2-G}{2+G}\right|+\frac{1}{4}\frac{V^2}{(G^2/2)-G}. \tag{B5}$$

Equations (B3)—(B5) guarantee particle conservation (see Ashcroft and Mermin[32]).

We now use

$$\int_0^{2\pi}d\varphi\frac{1}{a+i\delta+b\cos\varphi}=\frac{2\pi}{(a^2-b^2)^{1/2}}sgn(a)\Theta(a^2-b^2)-i\frac{2\pi}{(b^2-a^2)^{1/2}}\Theta(b^2-a^2) \tag{B6}$$

for $\delta\to 0^+$, with

$$\theta(u)=\begin{cases}1, & u>0\\ 0, & u<0\end{cases}$$

and $\operatorname{sgn}(a)=|a|/a$ and we then have

$$\mathrm{Re}\epsilon_{\vec{0}\,\vec{0}}(\vec{k},\omega)=1-\frac{3\omega_p^{0^2}}{16k^3}\left[\int_{-k_{F_1}}^{G/2}dp_{\|}\int_0^{[p_\perp^2(p_{\|})]_{1,\max}}dx\left[\frac{\mathrm{sgn}(\omega-k^2)\Theta([(\omega-k^2)/2k]^2-x)}{\{[(\omega-k^2)/2k]^2-x\}^{1/2}}-\frac{\Theta([\omega+k^2)/2k]^2-x)}{\{[(\omega+k^2)/2k]^2-x\}^{1/2}}\right]\right.$$
$$+\int_{G/2}^{k_{F_2}}dp_{\|}\int_0^{[p_\perp^2(p_{\|})]_{2,\max}}dx$$
$$\left.\times\left[\frac{\mathrm{sgn}(\omega-k^2)\Theta([(\omega-k^2)/2k]^2-x)}{\{[(\omega-k^2)/2]^2-x\}^{1/2}}-\frac{\Theta([(\omega+k^2)/2k]^2-x)}{\{[(\omega+k^2)/2k]^2-x\}^{1/2}}\right]\right] \tag{B7}$$

and

$$\mathrm{Im}\epsilon_{\vec{0}\,\vec{0}}(\vec{k},\omega)=\frac{3\omega_p^{0^2}}{16k^3}\left[\int_{-k_{F_1}}^{G/2}dp_{\|}\int_0^{[p_\perp^2(p_{\|})]_{1,\max}}dx\left[\frac{\Theta(x-[(\omega-k^2)/2k]^2)}{\{x-[(\omega-k^2)/2k]^2\}^{1/2}}-\frac{\Theta(x-[(\omega+k^2)/2k]^2)}{\{x-[(\omega+k^2)/2k]^2\}^{1/2}}\right]\right.$$
$$\left.+\int_{G/2}^{k_{F_2}}dp_{\|}\int_0^{[p_\perp^2(p_{\|})]_{2,\max}}dx\left[\frac{\Theta(x-[(\omega-k^2)/2k]^2)}{\{x-[(\omega-k^2)/2k]^2\}^{1/2}}-\frac{\Theta(x-[(\omega+k^2)/2k]^2)}{\{x-[(\omega+k^2)/2k]^2\}^{1/2}}\right]\right]. \tag{B8}$$

In the integrals in the above expressions for $\mathrm{Re}\epsilon_{\vec{0}\,\vec{0}}(\vec{k},\omega)$ and $\mathrm{Im}\epsilon_{\vec{0}\,\vec{0}}(\vec{k},\omega)$ we have $\Theta([(\omega-k^2)/2k]^2-x)$ and $\Theta([(\omega+k^2)/2k]^2+x)$ which need to be evaluated for $0<x<[p_\perp^2(p_{\|})]_{1,\max}$ and $-k_{F_1}<p_{\|}<G/2$ and for $0<x<[p_\perp^2(p_{\|})]_{2,\max}$ and $0<p_{\|}<k_{F_2}$, respectively. It is straightforward to notice that one may define different regions in $(\vec{k},\omega)$ space corresponding essentially to the regions in which the Θ functions or the limits of the $p_{\|}$ integration should change. In Fig. 15 we show the different regions in the particle-hole excitation spectrum for aluminum within degenerate perturbation theory and for the case in which $\vec{G}$ is perpendicular to $\vec{k}$.

In the region in which $\omega>k^2+2(E_F+V^2/G^2)^{1/2}\cdot k$ (or $\omega>k^2+2\alpha_1 k$, see Fig. 15), we have that

$$\mathrm{Re}\epsilon_{\vec{0}\,\vec{0}}(\vec{k},\omega)=1-\frac{3\omega_p^{0^2}}{16k^3}\left[\int_{-k_{F_1}}^{G/2}dp_{\|}\int_0^{[p_\perp^2(p_{\|})]_{1,\max}}dx\left[\frac{1}{\{[(\omega-k^2)/2k]^2-x\}^{1/2}}-\frac{1}{\{[(\omega+k^2)/2k]^2-x\}^{1/2}}\right]\right.$$
$$\left.+\int_{G/2}^{k_{F_2}}dp_{\|}\int_0^{[p_\perp^2(p_{\|})]_{2,\max}}dx\left[\frac{1}{\{[(\omega-k^2)/2k]^2-x\}^{1/2}}-\frac{1}{\{[(\omega+k^2)/2k]^2-x\}^{1/2}}\right]\right]$$
$$=1+\frac{3\omega_p^{0^2}}{8k^3}\left[(k_{F_1}+k_{F_2})k+\int_{-k_{F_1}}^{G/2}dp_{\|}\left[\{[(\omega-k^2)/2k]^2-[p_\perp^2(p_{\|})]_{1,\max}\}^{1/2}\right.\right.$$
$$\left.-\{[(\omega+k^2)/2k]^2-[p_\perp^2(p_{\|})]_{1,\max}\}^{1/2}\right]$$
$$+\int_{G/2}^{k_{F_2}}dp_{\|}\left[\{[(\omega-k^2)/2k]^2-[p_\perp^2(p_{\|})]_{2,\max}\}^{1/2}\right.$$
$$\left.\left.-\{[(\omega+k^2)/2k]^2-[p_\perp^2(p_{\|})]_{2,\max}\}^{1/2}\right]\right] \tag{B9}$$

and

$$\mathrm{Im}\epsilon_{\vec{0}\,\vec{0}}(\vec{k},\omega)=0\,. \tag{B10}$$

The above expressions can easily be shown to reduce to the electron-gas result when $V\to 0$. Also, $\mathrm{Re}\epsilon_{\vec{0}\,\vec{0}}(\vec{k},\omega)$ for $V\neq 0$ is easily evaluated numerically as only one-dimensional integrals are involved.

In any point of the $(\vec{k},\omega)$ space for $\vec{G}\perp\vec{k}$, $\mathrm{Re}\epsilon_{\vec{0}\,\vec{0}}(\vec{k},\omega)$, and $\mathrm{Im}\epsilon_{\vec{0}\,\vec{0}}(\vec{k},\omega)$ given by (B7) and (B8) can easily be

evaluated analogously. As another example, when $(\vec{k},\omega)$ belong to the region defined by $\omega<k^2+2\alpha_1 k$, $\omega>2\alpha_1 k-k^2$, and $\omega>k^2+2\alpha_2 k$ (see Fig. 15) we then have

$$\mathrm{Re}\epsilon_{\vec{0}\,\vec{0}}(\vec{k},\omega)=1+\frac{3\omega_p^{0^2}}{8k^3}\left[(k_{F_1}+k_{F_2})k+\int_{-k_{F_1}}^{p_1}dp_{\parallel}\{[(\omega-k^2)/2k]^2-[p_1^2(p_{\parallel})]_{1,\max}\}^{1/2}\right.$$
$$+\int_{p_2}^{G/2}dp_{\parallel}\{[(\omega-k^2)/2k]^2-[p_1^2(p_{\parallel})]_{1,\max}\}^{1/2}-\int_{-k_{F_1}}^{G/2}dp_{\parallel}\{[(\omega+k^2)/2k]^2-[p_1^2(p_{\parallel})]_{1,\max}\}^{1/2}$$
$$\left.+\int_{G/2}^{k_{F_2}}dp_{\parallel}\left[\{[(\omega-k^2)/2k]^2-[p_1^2(p_{\parallel})]_{2,\max}\}^{1/2}-\{[(\omega+k^2)/2k]^2-[p_1^2(p_{\parallel})]_{2,\max}\}^{1/2}\right]\right] \tag{B11}$$

and

$$\mathrm{Im}\epsilon_{\vec{0}\,\vec{0}}(\vec{k},\omega)=\frac{3\omega_p^{0^2}}{8k^3}\int_{p_1}^{p_2}dp_{\parallel}\{[p_1^2(p_{\parallel})]_{1,\max}-[(\omega-k^2)/2k]^2\}^{1/2} \tag{B12}$$

with p_1 and p_2 meaning the roots of $[p_1^2(p_{\parallel})]_{1,\max}=[(\omega-k^2)/2k]^2$.

Comparison between $\mathrm{Re}\epsilon_{\vec{0}\,\vec{0}}(\vec{k},\omega)$ and $\mathrm{Im}\epsilon_{\vec{0}\,\vec{0}}(\vec{k},\omega)$, $\vec{G}\perp\vec{k}$, with the free-electron-gas result is presented in Fig. 5 (see text) for $k/k_F=0.4$ and both calculations give essentially the same result, as already mentioned in Sec. II of the text.

[1]See, for example, H. Raether, in *Springer Tracts in Modern Physics,* edited by G. Höhler (Springer, New York, 1965).

[2]K. Sturm, Adv. Phys. **31**, 1 (1982).

[3]E-Ni Foo and J. J. Hopfield, Phys. Rev. **173**, 635 (1968).

[4]H. Boersch, J. Geiger, A. Imbusch, and N. Niedrig, Phys. Lett. **22**, 146 (1966).

[5]E. Petri and A. Otto, Phys. Rev. Lett. **34**, 1283 (1975).

[6]M. Urner-Wille, J. Phys. D **10**, 49 (1977).

[7]C. H. Chen and J. Silcox, Phys. Rev. B **16**, 4246 (1977).

[8]S. P. Singhal, Phys. Rev. B **14**, 2352 (1976).

[9]N. W. Ashcroft and K. Sturm, Phys. Rev. B **3**, 1898 (1971).

[10]A summary of the main results is given in L. E. Oliveira and K. Sturm, Solid State Commun. **51**, 591 (1984).

[11]J. Stiebling, Diploma thesis, University of Hamburg, 1978; see also H. Raether, *Springer Tracts in Modern Physics,* edited by G. Höhler (Springer, Berlin, 1980), Vol. 88, p. 82.

[12]H. Möller and A. Otto, Phys. Rev. Lett. **45**, 2140 (1980); **46**, 1707 (1981).

[13]K. Sturm, Phys. Rev. Lett. **46**, 1706 (1981).

[14]Reduced units, i.e., energies in units of the free-electron Fermi energy ϵ_F^0 and wave vectors in units of the free-electron Fermi wave vector k_F, are used throughout the paper.

[15]P. Vashishta and K. S. Singwi, Phys. Rev. B **6**, 875 (1972).

[16]N. Iwamoto, E. Krotscheck, and D. Pines, Phys. Rev. B **29**, 3936 (1984).

[17]G. Dresselhaus, M. S. Dresselhaus, and D. Beaglehole, in Proceedings of the Third Material Research Symposium, National Bureau of Standards, Gaithersburg, 1969 (unpublished).

[18]H. Bross, J. Phys. F **8**, 2631 (1978).

[19]P. C. Gibbons, Phys. Rev. B **23**, 2536 (1981).

[20]U. Fano, Phys. Rev. **124**, 1866 (1961).

[21]That the square-root singularity survives the $p_\perp$ integration is an artifact of our model. Small departures from the parallelism of the bands along $p_\perp$ modify the square-root singularity as was shown by K. Sturm and N. W. Ashcroft, Phys. Rev. B **10**, 1343 (1974). However, this does not affect the conclusions drawn from our calculation in any essential way.

[22]M. Urner-Wille and H. Raether, Phys. Lett. **58A**, 265 (1976).

[23]P. M. Platzman and P. Eisenberger, Phys. Rev. Lett. **33**, 152 (1974).

[24]H. J. Höhberger, A. Otto, and E. Petri, Solid State Commun. **16**, 175 (1975).

[25]P. E. Batson, C. H. Chen, and J. Silcox, Phys. Rev. Lett. **37**, 937 (1976).

[26]J. Stiebling and H. Raether, Phys. Rev. **40**, 1293 (1978).

[27]R. K. Kalia and G. Mukhopadhyay, Solid State Commun. **15**, 1243 (1974).

[28]G. Mukhopadhyay, R. K. Kalia, and K. S. Singwi, Phys. Rev. Lett. **34**, 950 (1975).

[29]W. Schülke, N. Nagasawa, and S. Mourikis, Phys. Rev. Lett. **52**, 2065 (1984).

[30]C. H. Chen, Phys. Status Solidi B **83**, 347 (1977).

[31]See, for example, W. Gröbner, and N. Hofreiter, *Integral Tables,* 2nd ed. (Springer, Vienna, 1957), Vol. 1.

[32]N. W. Ashcroft and N. D. Mermin, *Solid State Physics* (Holt, Rinehart, and Winston, Philadelphia, 1976).